Journal of Applied Science and Engineering, Vol. 21, No. 2, pp. 145–154 (2018) DOI: 10.6180/jase.201806_21(2).0001

Numerical Simulation of Scale Removal from Mine Drainage Pipe by Water Jet

Ziwei Zhang, Guoying Meng and Aiming Wang

School of Mechanical Electronic and Information Engineering, China University of Mining and Technology (Beijing), Beijing 100083, P.R. China

Abstract

To study the process of coal mine drainage pipe scale removal by using a water jet and its affecting parameters, a numerical model based on the fluid-solid interaction method is developed to simulate the removal process. The grid of the water jet and null material adopts ALE (Arbitrary Lagrange-Euler) formulation, while the pipe scale grid employs Lagrange formulation. The water jet penetration is simulated by coupling ALE fluid elements and Lagrange solid elements. The stress variation inside the pipe scale under the impact of water jet is analyzed. In addition, the effect of water jet parameters on the cutting depth is investigated. The numerical results are consistent with the experimental results. The results illustrate that the impact velocity and the incident angle of water jet have a significant influence on the impact depth determination. Small impact velocity causes erosion near the pipe scale surface and the actual crush occurs only when the velocity exceeds a certain value. The incident angle of water jet has an efficient range and larger cutting depths can be obtained as the incident angle increases up to 70°.

Key Words: Drainage Pipe Scale, Water Jet, ALE, Lagrange, Stress Variation, Cutting Depth

1. Introduction

The drainage pipeline is an important component of the coal mine drainage system in China. Majority of the drainage pipelines in the mines are relatively long and the mine water inside contains impurities such as coal slime. The impurities in mine water gradually deposit and solidify on the inner wall of the pipe after a certain period of drainage resulting in scale formation. Owing to the scale in the pipe, the hydraulic radius of the pipe is decreased and consequently the flow capacity is restricted. Moreover, severe scale induces unsafe production in the mines [1,2]. A section of drainage pipe scale sampled from a mine in China is shown in Figure 1. To ensure safe and efficient drainage, descaling should be conducted regularly. The water jet is a stream of dynamic fluid with highly concentrated energy, and it is widely utilized in the cleaning, cutting, breaking, and descaling of materials, as well as other engineering fields [3]. If the pipe robot carries water jet generator to run in the pipe, the water squirted from the generator can remove the scale in the pipe [4].

Since the process of water jet impacting the pipe

Figure 1. Coal mine drainage pipe scale.

*Corresponding author. E-mail: 751334315@qq.com

scale refers to nonlinear shock dynamics and it occurs in a short period of time, the breaking mechanism is complex and not yet comprehensible. In addition, the choice of proper process parameters has a significant influence on the descaling results, and it is difficult to demonstrate this process by utilizing the accurate analytical model [5–7].

A few researchers have conducted experiments to study and understand the nature of material destruction resulting from the water jet impact [8–10]; nevertheless, the possibilities of experimental study are limited with respect to the changes in the material body. In recent years, a couple of water jet researchers have adopted numerical approaches to investigate the sand-bed erosion, rock failure, radial tire rubber fracture, and metal deformation due to water jet impact. Tang et al. [11] investigated the sand-bed erosion behavior based on the computational fluid dynamics technique combined with the granular kinematic theory. The Eulerian algorithm is applied for the numerical simulation. Li [12] developed a numerical model to analyze the stress distribution inside the rock by the impingement of the water jet. The simulation is based on the utilization of the control volume method and the fully decoupled fluid-structure interaction theory. Jiang et al. [13] used the smoothed particle hydrodynamics (SPH) method to simulate the rock fragmentation process. Song et al. [14] studied the stress distribution of the rubber material under the impact of water jet and utilized the damage criterion to illustrate the fracture behavior of the tread rubber. Aganin [15] presented the computational results of an elastic-plastic body impacted by a high-velocity liquid jet. The dependence of the features of the body surface deformation on the body material is studied. These studies prove that the utilization of the numerical technique is an effective and favorable method. Based on the experimental analysis, the material property of the pipe scale is different from the above-mentioned materials, and therefore the predominant failure mechanism is also different [16–18].

The primary objective of the present study is to investigate the damage propagation and breaking mechanism of pipe scale impacted by a water jet. Furthermore, the process parameters exerting influence on the pipe scale removal is studied. The whole water jet impacting process is simulated by utilizing ANSYS/LS-DYNA software. The ALE algorithmis used to simulate the water and medium of air, and the Lagrangian algorithmis employed for modeling pipe scale. In addition, the dynamic fluid-structure interaction between water jet and the pipe scale is performed using a combination of the ALE and Lagrangian algorithms.

2. Arbitrary Lagrange-Euler (ALE) Formulation

The finite element calculation of the stress and strain of the materials usually adopts the Lagrange algorithm. In general, the deformation of the mesh is consistent with that of the material. However, it is known that the water jet impingement causes large deformation of water. The large deformation can contribute to severe mesh distortion, and the computation is probably terminated using the Lagrange method. The ALE method can describe the fluid in deformed domains and overcome the element distortion problem with high accuracy and efficient solution [19,20]. In terms of the mesh motion in the ALE approach, a reference coordinate, Lagrangian coordinates, and Eulerian coordinates are introduced. The fluid time derivative relative to the reference coordinate time derivative can be deduced as [21]:

$$\frac{\partial f(x_i,t)}{\partial t}+(v_i-u_i)\frac{\partial f(x_i,t)}{\partial x_i}=\frac{\partial f(X_i,t)}{\partial t} \tag{1}$$

where x_i is the Euler coordinates, X_i is the Lagrange coordinate, v_i is the fluid velocity, and u_i is the mesh velocity. The velocity and displacement of the fluid mesh are solved using conservation equations. The conservation equation for mass is illustrated as:

$$\frac{\partial \rho}{\partial t}=(-\rho)\frac{\partial v_i}{\partial x_i}-(v_i-u_i)\frac{\partial \rho}{\partial x_i} \tag{2}$$

where ρ is density.

The conservation equation for momentum is expressed as:

$$\rho\frac{\partial v_i}{\partial t}=\frac{\partial \sigma_{ij}}{\partial x_j}+\rho f_i-\rho(v_i-u_i)\frac{\partial v_i}{\partial x_j} \tag{3}$$

where σ_{ij} is the Cauchy stress [22], f_i is body force per unit mass, $i = 1, 2, 3, j = 1, 2, 3$.

The conservation equation for energy is shown as:

$$\rho \frac{\partial E}{\partial t} = \sigma_{ij} \frac{\partial v_i}{\partial x_j} + \rho f_i v_i - \rho (v_i - u_i) \frac{\partial E}{\partial x_j} \quad (4)$$

where E is internal energy per unit mass.

With respect to the solution of the ALE equations, two phases are involved at each time step. One or several Lagrangian time stepsare implemented during the first phase, where the mesh follows the material displacement to deform. Simultaneously, the distorted meshes are under constant boundary conditions. Further, the meshes are updated and the topologic relation of the mesh remains unchanged throughout the phase. In the second phase, the unit variables including mass, momentum and energy, and the nodal velocity vectors of the deformed mesh are transferred to the new mesh after remapping [23]. The numerical formulas which are for updating the velocity and displacement of each node are illustrated below:

$$\begin{cases} u^{n+1/2} = u^{n-1/2} + \Delta t M^{-1} (F_{ext} + F_{int}) x^{n+1} \\ x^{n+1} = x^{n-1} + \Delta t u^{n+1/2} \end{cases} \quad (5)$$

where f_{int} is the force inside element and F_{ext} is the force outside element. M is the mass matrix, $n = 0, 1, 2\ldots$

3. Numerical Model

3.1 Material Model for Water and Air

Material models make use of the constitutive equation together with the pressure derived by equation of state to resolve the internal characteristics of material. The fluid materials in numerical model incorporate water and air. The constitutive equationis employed to determine the relationship between the stress and strain and the state equationis used to describe the relationship between the pressure and volume respectively. In simulation, the constitutive model is based on the Null material model where the shear stiffness and the yield strength are ignored. Moreover, in Null material model, the deviatoric stress s_{ij} is proportional to strain rate $\dot{\varepsilon}_{ij}$, which is expressed as follows:

$$\sigma_{ij} = k \dot{\varepsilon}_{ij} \quad (i \neq j) \quad (6)$$

where k is the dynamic viscosity coefficient of fluid, the dynamic viscosity coefficient of air = 1.75 E-05 Pa · s, the dynamic viscosity coefficient of water = 8.68 E-05 Pa · s.

The Null material model combined with the linear polynomial equation of state is used with 1-point ALE multi-material element to model air in this paper. The equation of state is defined by the keyword *EOS_LINEAR_POLYNOMIAL in LS-DYNA, and its mathematical formula is expressed as follows:

$$p = C_0 + C_1\mu + C_2\mu^2 + C_3\mu^3 + (C_4 + C_5\mu + C_6\mu^2)e \quad (7)$$

where p is the pressure, e is the internal energy per unit volume, μ is the air volume ratio and it is calculated using the following formula:

$$\mu = \frac{\rho}{\rho_0} - 1 \quad (8)$$

where ρ is the compressed air density and ρ_0 is the air density before compression. The air is assumed as an ideal gas in this study, which can be expressed by setting:

$$C_0 = C_1 = C_2 = C_3 = C_6 = 0 \quad (9)$$

$$C_4 = C_5 = \gamma - 1 \quad (10)$$

where γ is the specific heat of air, $\gamma = C_p/C_v$, C_p is the specific heat capacity at constant pressure, and C_v is the specific heat capacity at constant volume.

The Null material model and the Gruneisen equation of state is used with 1-point ALE multi-material element to model water in this paper. The equation of state is defined by the keyword *EOS_GRUNEISEN in LS-DYNA and its mathematical formula is represented as:

$$p = \frac{\rho_0 C^2 \mu \left[1 + \left(1 - \frac{\gamma_0}{2}\right)\mu - \frac{a}{2}\mu^2\right]}{\left[1 - (S_1 - 1)\mu - S_2 \frac{\mu^2}{\mu + 1} - S_3 \frac{\mu^3}{(\mu + 1)^2}\right]^2} + (\gamma_0 + a\mu)e \quad (11)$$

where C is the longitudinal intercept for the curve of the shock wave velocity u_s versus the particle velocity u_P, S_1, S_2 and S_3 are the slope factors of the curve, γ_0 is the Gruneisen coefficient, and a is the first-order volume correction.

3.2 Material Model for Pipe Scale

The material model *MAT_PLASTIC_KINEMATIC is employed to describe the constitutive relation of the pipe scale in this study, which is material type 3 in LS-DYNA. It considers the elasto-plastic properties of the material and can evaluate the kinematic and isotropic hardening and the strain rate effects. Based on the experiment, the mechanical parameters of the scale in the mine drainage pipe are demonstrated as follows: density = 1224.5 kg/m^3, elastic modulus = 1.59 GPa, Poisson's ratio = 0.3, compressive strength = 4.3 MPa, Tensile strength = 0.67 MPa.

4. Explicit Finite Element Dynamic Analysis

The simulation model constitutes three components that include pipe scale, water, and air. The entire meshing utilizes the SOLID 164 element defined by eight nodes in LS-DYNA. The discretized dynamic equation for the simulation model based on the finite element method is defined as follows.

$$\boldsymbol{M}\ddot{\boldsymbol{x}}(t) = \boldsymbol{P}(t) - \boldsymbol{F}(t) + \boldsymbol{H}(t) - \boldsymbol{C}\dot{\boldsymbol{x}}(t) \tag{12}$$

where $\boldsymbol{M}$ is the mass matrix, $\boldsymbol{P}(t)$ is the nodal load vector, $\boldsymbol{F}(t)$ is the stress divergence vector, $\boldsymbol{H}(t)$ is the hourglass damping force vector, $\boldsymbol{C}$ is the damping matrix, and $\boldsymbol{x}(t)$ is the node coordinate vector.

The explicit central difference method is adopted to solve Eq. 12 and the recurrence formulations are shown as follows:

$$\begin{cases} \ddot{\boldsymbol{x}}(t_n) = \boldsymbol{M}^{-1}[\boldsymbol{P}(t_n) - \boldsymbol{F}(t_n) + \boldsymbol{H}(t_n) - \boldsymbol{C}\dot{\boldsymbol{x}}(t_{n-1/2})] \\ \dot{\boldsymbol{x}}(t_{n+1/2}) = \dot{\boldsymbol{x}}(t_{n-1/2}) + \ddot{\boldsymbol{x}}(t_n)(\Delta t_{n-1} + \Delta t_n)/2 \\ \boldsymbol{x}(t_{n+1}) = \boldsymbol{x}(t_n) + \dot{\boldsymbol{x}}(t_{n+1/2})\Delta t_n \end{cases} \tag{13}$$

where $\ddot{\boldsymbol{x}}(t_n)$ is the node acceleration vector at time t_n, $\dot{\boldsymbol{x}}(t_{n-1/2})$ is the node velocity vector at time $t_{n-1/2}$, and $\dot{\boldsymbol{x}}_{n+1/2}$ is the node velocity vector at time $t_{n+1/2}$.

Since water and air are involved in the process of water jet impacting the pipe scale, the multi-material ALE finite method is applied for the simulation. In addition, the formation of shock wave during the high-speed impact results in the discontinuity of pressure, density, particle acceleration, and energy, which makes it difficult to solve the dynamic equation. Therefore, we use an artificial volume viscosity term to correct the hydrostatic pressure. The artificial volume viscosity q is able to smooth the discontinuity of the shock wave with a continuous change in a sufficiently narrow region. With regard to the artificial volume viscosity term, the mathematical formula is defined as:

$$\begin{cases} q = \rho l\left(C_0 l\left|\dot{\varepsilon}_{kk}\right|^2 - C_1 a\left|\dot{\varepsilon}_{kk}\right|\right) & \dot{\varepsilon}_{kk} < 0 \\ q = 0 & \dot{\varepsilon}_{kk} \geq 0 \end{cases} \tag{14}$$

where the characteristic length $l = \sqrt[3]{v}$, a is the partial sound velocity, ρ is the density, the trace of strain rate tensor $\left|\dot{\varepsilon}_{kk}\right| = \left|(\dot{\varepsilon}_{11} + \dot{\varepsilon}_{22} + \dot{\varepsilon}_{33})\right|$, $C_0 = 1.5$, and $C_1 = 0.06$.

Considering the artificial volume viscosity term, the stress S_{ij} is calculated by:

$$S_{ij} = \sigma_{ij} + (p + q)\delta_{ij} \tag{15}$$

where p is the pressure and δ_{ij} is the kronecker delta.

5. Modeling Procedure

LS-DYNA solver can only run the K file that is exported by the preprocessor ANSYS, therefore geometric modeling, meshing and setting of simulation conditions need to be completed in ANSYS. Since some LS-DYNA keywords that are used in ALE simulation cannot be created by ANSYS, the K file is required to be re-edited and modified in order that we can apply ALE algorithm to conduct fluid structure interaction dynamic analysis. The ANSYS/LS-DYNA software is used to model and simulate the process of pipe scale removal. The primary procedures are demonstrated as follows.

5.1 Geometric Model and Boundary Condition

The process of establishing the geometric model is conducted in the graphical user interface (GUI) of ANSYS/LS-DYNA. The element type of the model is 3D164 that is used for explicit dynamic analyses. The geometric model of the pipe scale under water jet impact is shown in Figure 2. In Figure 2, component A is the water jet source, component B is the null material domain, and component C is the pipe scale. Component A is simplified as a column and its diameter is 4 mm. The height of component

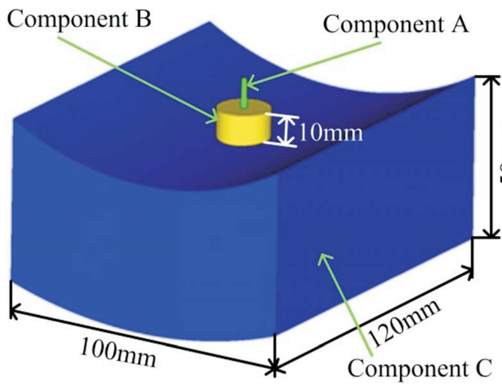

Figure 2. Geometric model of simulation.

B is 10 mm. The thickness of component C is 50 mm, its length is 120 mm and its width is 100 mm. The geometry of bottom and top of component C are constructed with curved surfaces, which is consistent with the actual specimens.

The finite element model is constituted by meshing the pipe scale domain and the fluid material domain respectively, which is illustrated in Figure 3. The mesh of components A and B is set to the ALE grid and component C is meshed using the Lagrange grid. The interaction of components A, B, and C is conducted by coupling the ALE and Lagrange grids. The mesh size applied in model affects the correctness of numerical results to some extent. In order to acquire proper size, a number of different mesh sizes are used to make the simulation model discretized. With the decrease of mesh size, the results obtained by simulations are able to better match the experimental values. As the mesh sizes of component A and B are less than 0.5 mm × 0.5 mm × 0.5 mm and the mesh size of component C is less than 2 mm × 2 mm × 1 mm, the numerical results are not varied any more and they approximate to experimental values. This indicates that the mesh size of 0.5 mm × 0.5 mm × 0.5 mm and 2 mm × 2 mm × 1 mm conforms to the requirement of correctness. The total number of element in whole model is 754360, and number of nodes is 771552.

For the boundary conditions, the bottom surface of component C is defined as fixed displacement condition, and non-reflecting conditions are applied to its surrounding surfaces where an unlimited domain is required.

5.2 Keyword Modification and LS-DYNA Solution

We set energy options, bulks viscosity, time step scale factor, solution time, number of steps, and other solver parameters in the GUI of ANSYS/LS-DYNA. After the option settings are accomplished, we output the keyword K file that is in ASC II format.

The keywords that are not produced in ANSYS should be written or modified in the K file. The major adjustments in the K file include: using the keyword *SECTION_SOLID_ALE to substitute the keyword *SECTION_SOLID and changing the default generated value of ELFORM to 11. The keyword *CONTROL_ALE is used, which is intended to control the ALE solution. Besides, to define two types of fluid material in the fluid field, the keyword *ALE_MULTI-MATERIAL_GROUP is generated. Furthermore, the keyword *CONSTRAINED_LANGRANGE_IN_SOLID is adopted to solve the fluid solid coupling, which is performed using the penalty function and the motion constraint algorithm. The modified K file is submitted to the LS-DYNA program for solution analysis.

6. Experimental Setup and Procedures

An electric powered water jet generator is used in the experiment, which is shown in Figure 4. The dimension of the machine is 1650 mm in length, 1100 mm in width and 1180 mm in height. The experimental setup mainly comprises a plunger pump, a PLC controller, an electric motor, a water jet nozzle, high pressure hoses, a water tank, a data acquisition system and a pressure sensor. The maximum water pressure and flow rate produced by the plunger pump are 50 MPa and 50 L/min respectively. The rated power of electric motor is 55 kW.

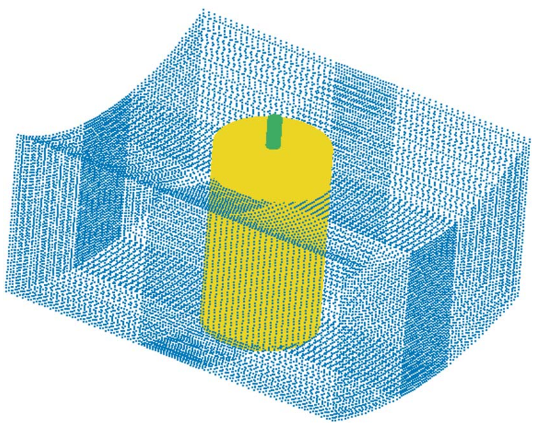

Figure 3. Meshing of the system.

Figure 4. Water jet generator.

The experiment focus on measuring the cutting depth of pipe scale subjected to water jet with different impact velocities. The diameter of nozzle used is the experiment is 4 mm and standoff distance is 10 mm in the experiment, which are consistent with numerical model. A number of experiments were conducted with the impact velocities ranging from 100 m/s to 250 m/s. The variation of impact velocity is regulated by changing the pressure of plunger pump. Each experiment is run for 20 s, and then stopping the plunger pump and measuring the cutting depth.

7. Results and Analysis

Figure 5 depicts the water jet impacting on the pipe scale in the initial stage. Figure 6 describes the status of the pipe scale under the water jet impact and the von-Misses stresses distribution inside the pipe scale at different time intervals. In this simulation, the included angle between the axis of the water jet and the pipe scale surface is 90°; the impact velocity is 200 m/s. It can be observed from Figure 6 that intensive stress is formed upon the edge of the hitting region. The maximum stress occurs in the zone closest to the edge. As the hitting proceeds, the high stress expands to the contiguous region. In addition, in the entire impacting process, the stress spreading domainis approximately uniform and the magnitude of stress is symmetric to the center of the impact zone. The depth of the material failure is also increased. Furthermore, the surrounding area of perforation is primarily subjected to the compressive stress.

Certain water jet parameters that influence the cut-

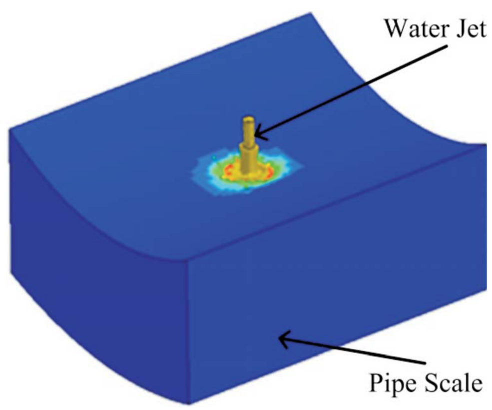

Figure 5. Water jet impacting on pipe scale in the initial stage.

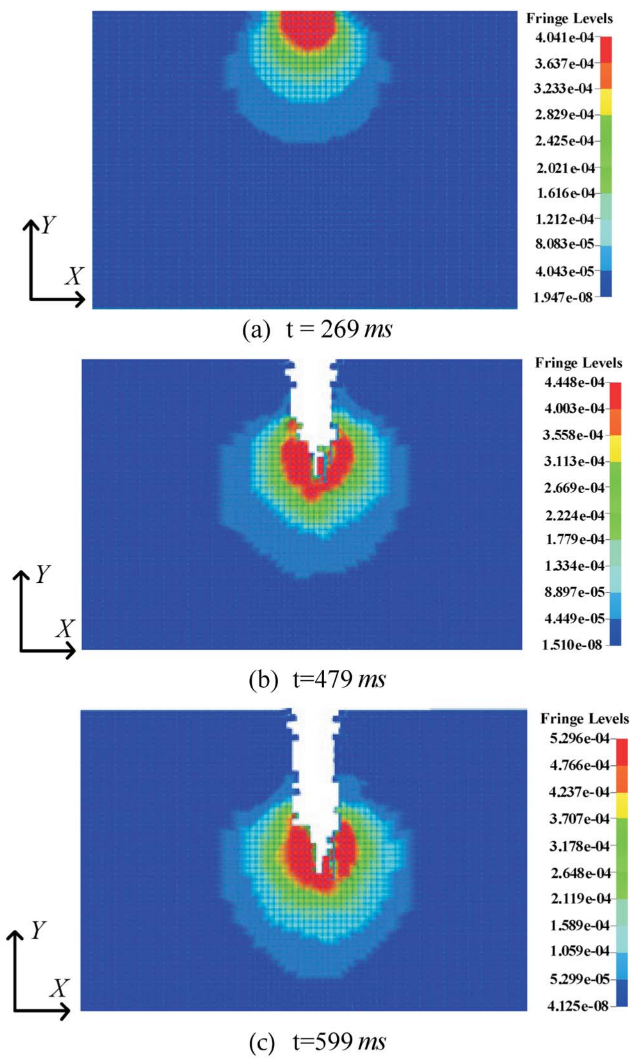

Figure 6. von Misses stresses within the pipe scale at a certain time stamp.

ting performances are investigated using a couple of simulations. In the following section, the impact velocity, incident angle, and breaking depth are discussed.

The velocity of the water jet determines the magnitude of the impact pressure on the pipe scale; hence, it exerts a key effect on the pipe scale removal. The simulation results of the cutting depth varying with the duration of water jet impact under different water jet velocity are illustrated in Figure 7. As shown in Figure 7, the cutting depth is increased continuously before 1.5 s. When the duration is more than 2 s, the rate of depth increment becomes constant. The relationship between the impact velocity and the cutting depth is demonstrated in Figure 8. Eight sets of velocities that vary from 100 m/s to 240 m/s are applied during the simulation and the numerical results are compared with that of the experiments. For each set of simulation and experiment, the duration is set to 10 s. It can be observed from Figure 8 that the extent of the pipe scale fragmentation is increased with the water jet velocity and the simulation results are satisfactorily in agreement with the experimental results. According to the results, two inflection values for the cutting depth vary with the impact velocity. When the impact velocity is V_1 (V_1 = 100 m/s), the impact pressure is small, which limits the damage range and only a small crush pitis formed on the surface. When the impact velocity is V_2 (V_2 = 163 m/s), the breaking depth is rapidly increased. The increment rate of breaking depth becomes moderated over time when the impact velocity is greater than 180 m/s. The overall trend of increment of breaking depth is non-linear but step-like type and the amount of increase rate is the largest when the impact velocity is between 163 m/s and 180 m/s. Figures 9 and 10 show the breaking status of the pipe scale at 3 s with the impact velocities equal to 100 m/s and 163 m/s respectively. Based on the results shown in the two figures, it can be inferred that the lower impact velocity results in the erosion of the pipe and the actual crush occurs as the velocity exceeds a certain magnitude.

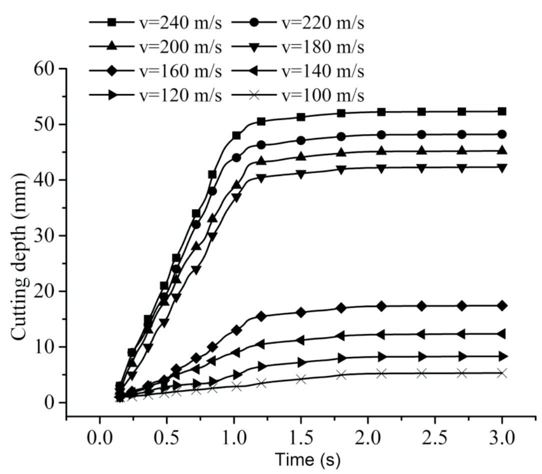

Figure 7. Variation of cutting depth over time under different water jet velocities.

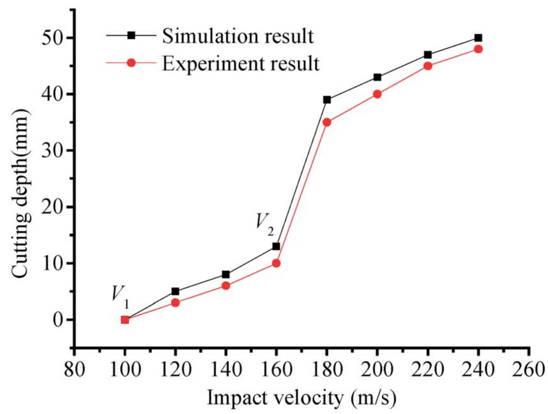

Figure 8. Relationship between impact velocity and cutting depth.

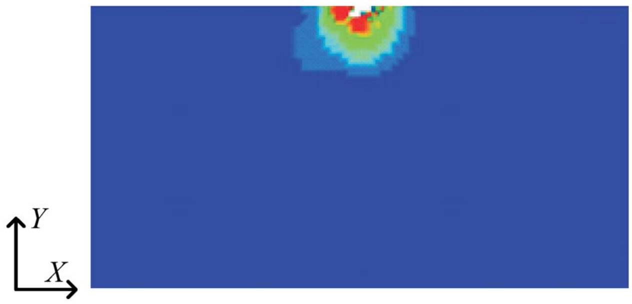

Figure 9. Breaking status of pipe scale as the impact velocity is 100 m/s.

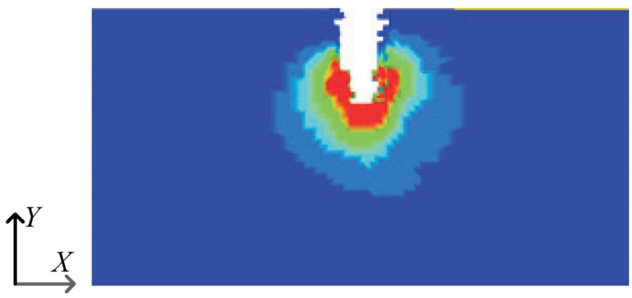

Figure 10. Breaking status of pipe scale as the impact velocity is 163 m/s.

The incident angle is formed by the axis of water jet and the surface of pipe scale. Six different incident angles of 40°, 50°, 60°, 70°, 80°, and 90° are utilized in the simulation with the water jet velocity equal to 250 m/s. The results of the cutting depth varying with time are demonstrated in Figure 11. It can be observed from Figure 11 that pipe scale breaks at the initial period of 0.3 s to 1 s. As the period of water impact is over 1 s, the increment rate of cutting depth is diminished greatly. Consequently, the water jet impacting duration makes no effect on the cutting depth after 1 s in simulations. Figure 12 illustrates the extent of the cutting depth at time 1 s with different incident angles. According to Figure 12, the general variation trend is that the cutting depth increases approximately linearly with the increase of incident angle, except that a small increment trend variation occurs at incident angle equal to 60°. On the other hand, this also indicates that the incident angle is one of the important parameters affecting the water jet damage and rock breaking. When the incident angle is below 40°, the jet impact energy cannot effectively damage the pipe scale with oblique impact as a result of hydrodynamic friction coefficient, which results in a small crushing. When the incident angle is up by 70°, the cutting depth of the pipe scale is sufficiently larger since the damage capability of the stress wave is increased. Based on the above analysis, the pipe scale crushing effect is better when the incident angle is larger than 70°.

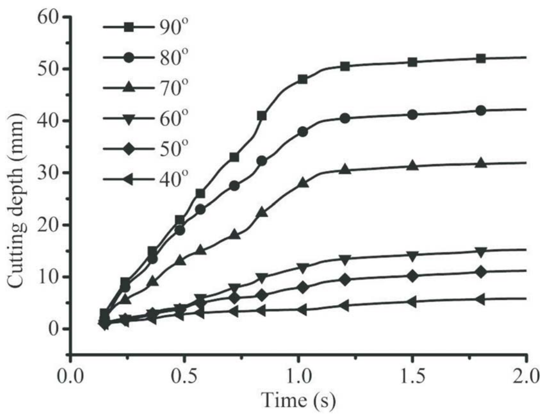

Figure 11. Variations of cutting depth over time under different incident angles.

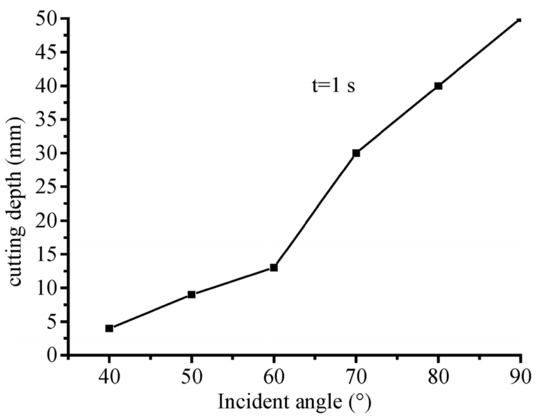

Figure 12. Relationship between incident angle and cutting depth.

8. Conclusions

The model of the pipe scale impacted by water jet is established using the ALE algorithm. Based on the simulation and experimental results, we can deduce the following conclusions.

1. The stress concentration occurs around the contact region between the water jet and the pipe scale. With continuous impact, the stress expands as a wave. In the entire process, the shape of the stress region remains basically the same, and the maximum stress region is symmetrically distributed.
2. The impact velocity and the incident angle exert critical effect on the cutting of the pipe scale by a water jet. When the jet velocity is small, the damage of the pipe scale is dominated by erosion. The pipe scale is effectively crushed as the impact velocity attains a certain value. The velocity for effective impact is up to 163 m/s. There is an optimal range for the incident angle of the water jet when impinging on the pipe scale. The pipe scale crushing effect is better as incident angle exceeds 70°.

Acknowledgements

The authors would like to thank the Henan Energy Chemical Industry Group Limited Company for their financial support in the work.

References

[1] Vijaykumar, R., Julie, M. J., Vieira, A. T., Humphrey, J. and Zheng, D., "Startup and Shutdown Steam Gen-

erator Separator Piping Forces for a Coal-fired Supercritical Power Plant," Proc of the ASME 2012 Pressure Vessels and Piping Conf, Toronto, Ontario, Vol. 3, pp. 7011−707 (2012). doi: 10.1115/PVP2012-78798

[2] Han, Q. Y., Peng, X. and Yang, Y. P., "Influence of Emulsion on the Corrosion and Scaling on Pipelines of Cooling System Deep Coal Mine: a Experiment Study," *Advanced Materials Research*, Vol. 902, No. 3, pp. 105−110 (2014). doi: 10.4028/www.scientific.net/ARM.902.105

[3] Lu, Y. Y., Huang, F., Wang, J. H. and Liu, X. C., "Analysis of Stress Wave Effect During Rock Breakage Process by Ultra-high Pressure Water Jet," *Journal of China University of Mining & Technology*, Vol. 42, No. 4, pp. 519−525 (2013).

[4] Wang, C. J., "Design of Pipe Scale Removal Robot for Coal Mine Pipe," *Coal Mine Machinery*, Vol. 30, No. 8, pp. 24−26 (2009). doi: 10.13436/j.mkjx.2009.08.050

[5] Hsu, C. Y., Liang, C. C., Teng, T. L. and Nguyen, A. T., "A Numerical Study on High-speed Water Jet Impact," *Ocean Engineering*, Vol. 72, No. 1, pp. 98−106 (2013). doi: 10.1016/j.oceaneng.2013.06.012

[6] Junkar, M., Jurisevic, B., Fajdiga, M. and Grah, M., "Finite Element Analysis of Single-particle Impact in Abrasive Water Jet Machining," *Int. J. Impact Eng.*, Vol. 32, No. 2, pp. 1095−1112 (2006). doi: 10.1016/j.ijimpeng.2004.09.006

[7] Lebar, A. and Junkar, M., "Simulation of Abrasive Waterjet Machining Based on Unit Event Features," *Proc. Inst. Mech. Eng. B. J. Eng. Manuf.*, Vol. 217, No. 25, pp. 699−703 (2003). doi: 10.1243/095440503322011425

[8] Chahine, G. L. and Kalumuck, K. M., "The Influence of Structural Deformation on Water Jet Impact Loading," *J. Fluids Struct.*, Vol. 12, No. 1, pp. 103−121 (1998). doi: 10.1006/jfls.1997.0127

[9] Lu, Y. Y., Huang, F., Liu, X. C. and Ao, X., "On the Failure Pattern of Sandstone Impacted by High-velocity Water Jet," *Int. J. Impact Eng.*, Vol. 76, No. 3, pp. 64−74 (2015). doi: 10.1016/j.ijimpeng.2014.09.008

[10] Lee, J. H., Park, K. S., Kang, M. C., Kang, B. S. and Shin, B. S., "Experiments and Computer Simulation Analysis of Impact Behaviors of Micro-sized Abrasive in Waterjet Cutting of Thin Multiple Layered Materials," *Trans. Nonferrous Met. Soc. China*, Vol. 22, No. 3, pp. 864−869 (2012). doi: 10.1016/S1003-6326(12)61817-2

[11] Tang, Y., Chan, D. H. and Zhu, D. Z., "Numerical Investigation of Sand-bed Erosion by an Upward Water Jet," *J. Eng. Mech.*, Vol. 143, No. 9, pp. 1−14 (2015). doi: 10.1061/(ASCE)EM.1943-7889.0001319

[12] Li, G. S., Liao, H. L., Huang, Z. W. and Shen, Z. H., "Rock Damage Mechanisms under Ultra-high Pressure Water Jet Impact," *Journal of Mechanical Engineering*, Vol. 45, No. 10, pp. 284−293 (2009). doi: 10.3901/JME.2009.10.284

[13] Jiang, H. X., Liu, Z. H. and Gao, K. D., "Numerical Simulation on Rock Fragmentation by Discontinuous Water-jet Using Coupled SPH/FEA Method," *Powder Technol.*, Vol. 312, No. 10, pp. 248−259 (2015). doi: 10.1016/i.powtec.2017.02.047

[14] Song, S. X., Tian, G. T. and Yu, D. Q., "Fracture Mechanism of Radial Tyre Rubber under Ultra-high Pressure Water Jet Impact," *Journal of Mechanical Engineering*, Vol. 50, No. 12, pp. 36−43 (2014). doi: 10.3901/JME.2014.12.036

[15] Aganin, A. A. and Khismatullina, N. A., "Features of Deformation of Metal Body Surfaces under Impact of a Water Jet," *Journal of Physics Conference Series*, Vol. 669, No. 2, pp. 1−4 (2016). doi: 10.1088/1742-6596/669/1/012031

[16] Brunton, J. H., "High Speed Liquid Impact," *Phil. Trans. A*, Vol. 260, No. 3, pp. 79−85 (1966). doi: 10.1088/1742-6596/669/1/012031

[17] Ahmed, D. H., Naser, J. and Deam, R. T., "Particle Impact Characteristics on Cutting Surface During the Abrasive Water Jet Machining: Numerical Study," *J. Mater. Process. Technol.*, Vol. 232, No. 10, pp. 116−130 (2016). doi: 10.1016/j.jmatprotec.2016.01.032

[18] Li, R., Ninokata, H. and Mori, M., "A Numerical Study of Impact Force Caused by Liquid Droplet Impingement onto a Rigid Wall," *Prog. Nucl. Energy*, Vol. 53, No. 10, pp. 881−885 (2011). doi: 10.1016/j.pnucene.2011.03.002

[19] Aquelet, N., Souli, M. and Olovsson, L., "Euler-Lagrange Coupling with Damping Effects: Application to Slamming Problems," *Comput. Methods Appl. Mech. Engrg*, Vol. 195, No. 9, pp. 110−132 (2006). doi: 10.1016/j.cma.2005.01.010

[20] Sheng, D. C., Nazem, M. and Carter, J. P., "Some Computational Aspects for Solving Deep Penetration Problems in Geomechanics," *Comput. Mech.*, Vol. 44, No. 10, pp. 549−561 (2009). doi: 10.1007/s00466-009-0391-6

[21] Souli, M. and Shahrour, I., "Arbitrary Lagrangian Eulerian Formulation for Soil Structure Interaction Problems," *Soil Dynamics and Earthquake Engineering*, Vol. 35, No. 3, pp. 72−79 (2012). doi: 10.1016/j.soildyn.2011.10.006

[22] Kim, J. H. and Shin, H. C., "Application of the ALE Technique for Underwater Explosion Analysis of a Submarine Liquefied Oxygen Tank," *Ocean Engineering*, Vol. 35, No. 10, pp. 812−822 (2008). doi: 10.1016/j.oceaneng.2008.01.019

[23] Movahhedy, M. R., Gadala, M. S. and Altintas, Y., "Simulation of Chip Formation in Orthogonal Metal Cutting Process: an ALE Finite Element Approach," *Machining Science and Technology*, Vol. 1091, No. 344, pp. 15−45 (2000). doi: 10.1080/10940340008945698

Manuscript Received: Mar. 7, 2018
Accepted: Apr. 16, 2018